Terahertz polariton sidebands generated by ultrafast strain pulses in an optical semiconductor microcavity

T. Berstermann,[1] A. V. Scherbakov,[2] A. V. Akimov,[2] D. R. Yakovlev,[1,2] N. A. Gippius,[3,4] B. A. Glavin,[5] I. Sagnes,[6] J. Bloch,[6] and M. Bayer[1]

[1]*Experimentelle Physik 2, Technische Universität Dortmund, D-44227 Dortmund, Germany*

[2]*A.F. Ioffe Physico-Technical Institute, Russian Academy of Sciences, 194021 St. Petersburg, Russia*

[3]*LASMEA, UMR 6602 CNRS, Université Blaise Pascal, 24 Avenue des Landais, 63177 Aubière, France*

[4]*A.M. Prokhorov General Physics Institute, RAS, 119991 Moscow, Russia*

[5]*Institute of Semiconductor Physics, National Academy of Sciences, Kiev 03028, Ukraine*

[6]*Laboratoire de Photonique et de Nanostructures, LPN/CNRS, Route de Nozay, 91460 Marcoussis, France*

(Received 7 July 2009; published 3 August 2009)

We apply ultrafast optical and acoustic techniques to a semiconductor quantum well microcavity in the strong-coupling regime. By injecting terahertz strain pulses a modulation domain can be obtained in which large variations in the optical frequency are induced on time scales shorter than the polariton decoherence. Under these conditions characteristic sidebands which are spectral fingerprints of the terahertz modulation process appear in the spectrum near the polariton resonance.

DOI: 10.1103/PhysRevB.80.075301 PACS number(s): 78.20.Hp, 78.67.De

I. INTRODUCTION

Manipulation on ever faster time scales has led to enormous progress in basic and applied research. These advancements in ultrafast control have been based mostly on the availability of ultrafast laser sources, which may provide coherent light pulses with durations as short as attoseconds. In parallel the field of ultrafast acoustics has been developed, which exploits elastic vibrations in solids at terahertz (THz) and sub-THz frequencies. The ultrafast acoustics techniques developed during the last two decades have enabled the generation of picosecond strain pulses, wave packets,[1,2] and acoustic solitons,[3] as well as observation of THz harmonic elastic oscillations in superlattices[4,5] or phonon microcavities[6] and stimulated emission of THz phonons.[7]

Recently efforts have been undertaken to merge the fields of ultrafast optics and acoustics resulting in a variety of novel acousto-optic phenomena. Among them are the generation of THz radiation by acoustic waves,[8] the amplification of THz sound waves in a combined optical and phonon microcavity,[9] and strain pulse induced chirping of an optical transition.[10]

It is well-known that traditional MHz and GHz acoustics allows efficient modulation of the optical frequency ω such that the variations $\Delta\Omega$ of the modulation amplitude are large enough to be seen in the spectrum of the optical signal.[11,12] When the modulation of the signal occurs on a time scale τ_a (the time that it takes the optical frequency to reach maximum modulation $\Delta\Omega$) which is much longer than the coherence time τ_c, it is easily possible to follow the time dependence of the modulated optical frequency $\omega(t)$ from the light intensity, as the modulation occurs adiabatically. For semiconductors, for example, modulation frequencies τ_a^{-1} in the GHz regime could be achieved corresponding to τ_a exceeding by far the typical coherence times $\tau_c \sim 10^{-12}-10^{-11}$ s in these systems. In this case the existing time-resolved methodologies using linear or nonlinear spectroscopy are fully sufficient to track $\omega(t)$.

Tracing the optical frequency modulation $\omega(t)$ from the spectrum is hampered, however, when τ_a is clearly shorter than τ_c and simultaneously the perturbation is so strong that the modulation amplitude $\Delta\Omega$ exceeds by far the stationary spectral width $\Delta\omega \sim \tau_c^{-1}$. This appealing situation is implemented here for an optical-model system for which the adiabatic regime is left by applying an ultrafast acoustic technique. The nonadiabatic situation, with which one is confronted then, is characterized by

$$\tau_a \leq \tau_c, \quad \Delta\Omega > \Delta\omega. \tag{1}$$

In detail, we apply ultrafast strain pulses to a semiconductor microcavity (MC) in the strong-coupling regime showing coherent emission over comparatively long times. Insight in the nonadiabatic regime can be taken by analyzing the optical signal in the spectral domain. At first glance, such a spectral analysis appears to be inappropriate as all information about the modulation process should be blurred by signal integration over times essentially longer than τ_a. In contrast, we show experimentally that the spectrum contains clear signatures of the microcavity resonance modulation. In agreement with a theoretical model we demonstrate that in the nonadiabatic regime pronounced sidebands of the modulated resonance appear from which information about the modulation process can be obtained.

II. EXPERIMENT

The basic scheme of the experiments which were carried out at liquid-helium temperature ($T=1.8$ K) is shown in Fig. 1. The high finesse optical MC structure [panel (a)] contains an 8-nm-wide $In_{0.04}Ga_{0.96}As$ quantum well (QW) in the middle of a GaAs barrier layer with width $d=240$ nm, corresponding to the wavelength λ of the confined photon resonance. This λ-cavity layer is surrounded by distributed Bragg reflectors made from 24 and 20 pairs of GaAs/AlAs $\lambda/4$ stacks at the bottom (toward substrate) and the top (toward

 ©2009 The American Physical Society

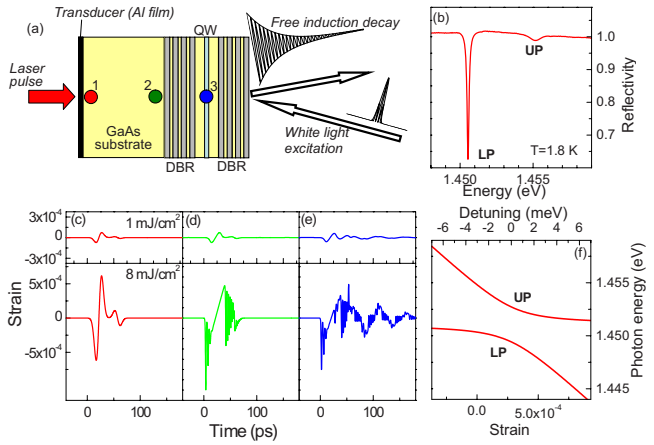

FIG. 1. (Color online) Experimental principles of modulation. (a) Scheme of the experiments on a microcavity formed by two distributed Bragg reflector mirrors (DBR) with a quantum well embedded in between. The strain pulses are generated by a laser pulse, shown by the red arrow (left side), focused onto an Al film. (b) Reflectivity spectrum from the MC without applied modulation. LP and UP correspond to the spectral resonances of the lower and upper polaritons, respectively. (c–e) Strain pulses $\varepsilon(t)$ simulated for low (upper panels) and high (lower panels) excitation densities W at various distances (indicated by the spots *1–3* in panel (a) from the Al transducer. The propagation time from the transducer to the corresponding points was subtracted for clarity. (f) Dependencies of UP and LP energies in the MC as function of static strain (lower scale) and detuning between the energies of the uncoupled photon mode and exciton state (upper scale).

vacuum), respectively. The Q factor of the MC is $\sim 10^4$, which is large enough to reach the strong-coupling (polariton) regime between the QW exciton state and the confined photon mode.[13,14] Figure 1(b) shows the stationary optical reflectivity spectrum $R(E)$ of the MC in which two narrow resonances corresponding to the lower (LP) and upper (UP) polaritons are seen. The photonlike LP resonance is slightly broadened relatively to the cavity mode due to the mixing with the inhomogeneously broadened exciton state and has a spectral width $\Delta\omega = 0.18$ meV.

In the ultrafast coherent experiments the polariton resonances were excited by 150 fs white light pulses from a laser system with a repetition rate 100 kHz. The beam was focused on the sample surface of the MC to a spot with diameter 100 μm. The excitation density did not exceed 50 nJ/cm^2. As a result of the femtosecond broadband excitation the LP and UP states emit coherent light into the specular direction relative to the excitation beam [Fig. 1(a)]. This coherent emission decaying with time τ_c is known as optical free-induction decay.[15] The value of τ_c is connected with the spectral width of the resonance $\Delta\omega$ by the following relation:

$$\tau_c = \frac{2}{\Delta\omega}. \tag{2}$$

The factor 2 arises from the fact that τ_c corresponds to the decay of the electromagnetic field amplitude, while the spectral width of the optical resonance reflects the decay of the field intensity. The value of τ_c for the LP resonance obtained by Eq. (2) from the optical spectrum is equal to 7.2 ps.

The THz frequency modulation in our experiments is achieved using strain pulses injected into the sample by ultrafast acoustics methods.[1,2] Picosecond strain pulses are generated by excitation of a 100-nm-thick Al film deposited on the GaAs substrate opposite to the MC by 800-nm-femtosecond light pulses taken from the same laser system as the white light pulse [Fig. 1(a)]. As a result of the photoexcitation the film expands rapidly due to the thermoelastic effect and a bipolar strain pulse is injected into the substrate [Fig. 1(c)]. In our experiments the initial strain pulse injected into the substrate has a total duration of ~ 70 ps.[1,16] The energy density of the excitation pulse could be increased up to $W = 16$ mJ/cm^2, which corresponds to a maximum strain amplitude of $\eta_0 \sim 10^{-3}$.[10,17]

The strain pulses propagate through the 100 μm GaAs substrate at the velocity $c_{LA} \approx 4.8 \times 10^3$ m/s of longitudinal sound in GaAs.[18] Accordingly the strain pulses reach the MC with a delay of about 20 ns relative to the 800-nm excitation pulse. The temporal shape of the strain pulse reaching the MC strongly depends on the excitation density. At low excitation densities $W < 1$ mJ/cm^2 the shape does not change much while propagating through the substrate [compare upper panels (c) and (d)]. At higher W nonlinear elasticity and phonon dispersion become important and the shape is modified during propagation due to formation of a shock wave and, at low temperatures, an acoustic soliton train at the beginning of the strain pulse, while at its end dispersive phonon oscillations take place.[3] The temporal evolution of the strain pulse for this nonlinear regime, shown in the lower panel of Fig. 1(d), was calculated numerically as described in Ref. 3. Further modifications [Fig. 1(e)] of the strain pulse reaching the QW are due to multiple reflections at the interfaces of the MC structure.[19]

The strain pulse $\eta(t)$ arriving at the QW modulates the detuning $\Delta E = E_{MC} - E_X$ between the energies of the uncoupled cavity mode and exciton, E_{MC} and E_X, respectively. The effect of the strain pulse on E_X is significantly stronger than on E_{MC}.[20] Strain induces a time-dependent detuning $\Delta E(t) = \tilde{a}\eta(t) + \Delta E_0$, where $\tilde{a} \sim -10$ eV is the deformation potential of the exciton in the (In,Ga)As/GaAs QW (Refs. 21 and 22) and ΔE_0 is the detuning without strain pulse. Using the dependence of the polariton energy on the detuning [Fig. 1(f)] we may estimate the corresponding energy shift in the polariton resonances within the coherence time τ_c. For instance in the time interval 10 ps $< t <$ 25 ps we expect a shift in the LP resonance within $\tau_c = 7.2$ ps by 0.15 meV for $W = 1$ mJ/cm^2 and 0.37 meV for $W = 8$ mJ/cm^2. Thus the effect of a strain pulse with sufficient amplitude on the polariton resonance energies turns out to be well suited to reach a nonadiabatic optical modulation at THz frequencies which fulfils the conditions set by Eq. (1).

III. RESULTS AND QUALITATIVE MODEL

In the experiments, the spectrum of the coherent polariton emission was analyzed by a spectrometer with a resolution of 0.15 meV and monitored as function of the time delay t_0

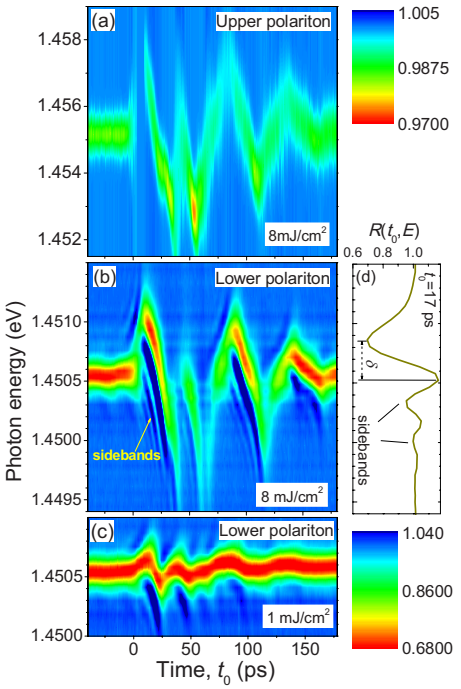

FIG. 2. (Color online) Experimental spectral/temporal contour plots. The modulated UP (a) and LP (b, c) optical signals measured at high (a, b) and low (c) excitation densities W focused onto the hypersonic transducer. Panels (b) and (c) have the same intensity scale, which is shown on the right of (c). (d) Spectrum measured at delay $t_0=17$ ps between the arrival of the strain pulse at the MC and the white light pulse.

between the white light excitation pulse and the strain pulse at the QW. The results are shown in Fig. 2 for the UP [panel (a)] and LP [panels (b) and (c)]. Clearly the polariton spectrum, which under stationary conditions consists of the well defined UP and LP resonances [Fig. 1(b)], undergoes enormous changes when the strain pulse is hitting the QW. THz modulation of the UP energy [panel (a)] by several meV occurs. Regardless of the smaller LP modulation amplitude [panels (b) and (c)], for certain values of delay t_0 the LP spectra show a remarkable, well defined structure with spectral fringes at the flanks of the main resonance. The most pronounced sidebands with up to three fringes are observed for high amplitude strain pulses [panel (b)] in the delay intervals $t_0=10-25$ ps and $t_0=90-105$ ps, which correspond to the linear parts of the strain evolution [lower panel (e) of Fig. 1]. Figure 2(d) shows the reflectivity spectrum $R(t_0,E)$ for a delay $t_0=17$ ps, at which several fringes are clearly detected.

We associate the experimentally observed spectral sidebands with the specifics of the nonadiabatic THz optical frequency modulation. To illustrate that this observation is a general phenomenon we consider a scalar harmonic oscillator decaying with time τ_c which can be described by a time-dependent variable $x(t)$ following the equation of motion:

$$\frac{d^2x}{dt^2} = -\omega_0^2(t)x - \frac{2}{\tau_c}\frac{dx}{dt} + f(t-t_0), \tag{3}$$

where $\omega_0(t)$ is its time varying frequency and $f(t-t_0)$ is a short excitation pulse acting on the oscillator at time $t=t_0$. In

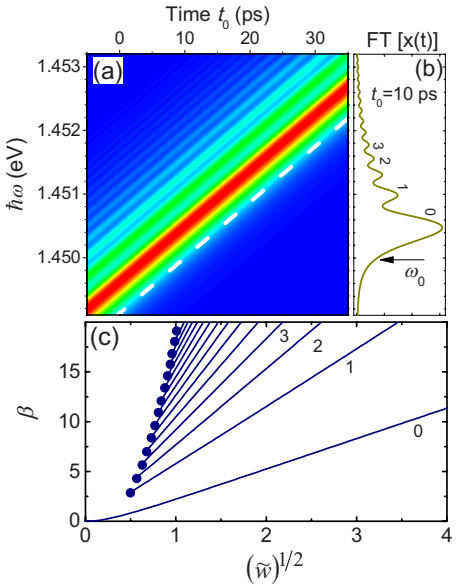

FIG. 3. (Color online) Calculations of the modulated spectrum of a scalar oscillator excited by a broad band excitation pulse in a situation when the resonance energy changes linearly with time: (a) spectral/temporal contour plot of the power Fourier-transformed time-dependent variable x, ω_0 (t_0) is shown by the dashed line; (b) oscillator power spectrum for $t_0=10$ ps; (c) normalized positions γ of the sideband maxima as function of the parameter $\tilde{w}$, which characterizes the modulation rate. Symbols indicate the values below of which the corresponding maximum cannot be observed.

our experiments $\omega_0(t)$ and $f(t-t_0)$ are associated with the polariton optical frequency and white light excitation, respectively, where $x(t)$ is the polariton field. The Fourier-transformed (FT) power spectrum of $x(t)$ for the case when $\omega_0(t)$ is increasing linearly with t is shown in the contour plot in Fig. 3(a) as function of t_0. We have chosen scales, values, and initial conditions for solving Eq. (3) in accordance with the experiments. A high-energy sideband with well resolved spectral fringes is clearly seen. The sidebands can be also seen in Fig. 3(b) which shows the spectrum obtained at a fixed delay of $t_0=10$ ps. Besides these sidebands, the typical feature in the time-integrated spectra for delay t_0 is the shift in the spectral density maximum to higher energies with respect to $\omega_0(t)$ which is shown in Fig. 3(a) by the dashed white line. In the case when $\omega_0(t)$ is decreasing with t_0 the spectral density maximum is shifted to lower energies relative to $\omega_0(t)$ and the sidebands appear on the low-frequency side of the stationary resonance position.

Figure 3(c) shows the normalized positions $\gamma=\tau_c(\tilde{\omega}_m-\omega_0)$ of the sideband maxima of the modulated signal at frequencies $\tilde{\omega}_m$ $(m=0, 1, 2\ldots)$ as a function of the dimensionless parameter $\tilde{w}=\tau_c^2(d\omega_0/dt)$, which is the ratio of the frequency shift during the coherence time τ_c and the half of the resonance's spectral width τ_c^{-1}. The maxima positions are seen to be proportional to $(\tilde{w})^{1/2}$. The symbols indicate the values of $\tilde{w}$ below which the corresponding fringe does not show up as a maximum in the spectrum. From Fig. 3(c) the value should be higher than 0.5 to have at least one additional maximum. According to the theory the sidebands in our experiments will become well pronounced if the shift

in a polariton resonance within the coherence time τ_c exceeds $\Delta\omega/8=0.0225$ meV. Such conditions are obviously realized in the detected signals shown in Fig. 2.

IV. NUMERICAL ANALYSIS

The model presented above demonstrates the general idea of the nonadiabatic approach. To become more quantitative, a specific analysis has been done for the MC studied here.

The strain pulse results in a time-dependent modulation of the exciton energy $E_X(t)$, which is observed as a shift in the polariton resonances in the strong-coupling regime. Because the amplitude of the exciton shift $\delta E_X(t)$ exceeds the polariton Rabi splitting the adequate description cannot be obtained within the single (lower or upper) polariton branch approximation. Instead direct solution of the Maxwell equations with a time dependent exciton resonance is necessary. If the spectral range of interest is narrow compared to the stop band of the cavity Bragg mirrors the resonant approximation of cavity electrodynamics can be used.[23,24] This approximation greatly speeds up the calculations while at the same time providing reasonable accuracy. Within this approximation the Maxwell equations are reduced to a system of two coupled equations that describe the dynamics of the cavity mode electric field at the quantum well $\mathcal{E}_{QW}(k,t)$

$$\left[i\frac{d}{dt}-E_{MC}(k)\right]\mathcal{E}_{QW}(k,t)=\beta(k)\sum_i P^i(k,t)+\alpha(k)\mathcal{E}_{\mathrm{inc}}(k,t), \tag{4}$$

and of the resonant exciton polarization, integrated over the thickness of the quantum well $P(k,t)$

$$\left[i\frac{d}{dt}-E_X^i(t)\right]P^i(k,t)=A^i\mathcal{E}_{QW}(k,t). \tag{5}$$

Here E_{MC} and E_X are the resonance energies with nonzero imaginary parts due to the decay of the cavity mode and exciton dephasing, respectively. A is the magnitude of the quantum well exciton resonance susceptibility, α and β are the coupling constants of the microcavity electromagnetic field with the external field and the QW exciton polarization, respectively. The cavity polariton Rabi splitting (Ω_R) can be calculated by $\Omega_R=\sqrt{A\beta}$. The incident pulse far from the microcavity $\mathcal{E}_{\mathrm{inc}}(k,t)=\mathcal{E}(t)\exp(-i\Omega_{\mathrm{inc}}t)\delta(k-k_{\mathrm{inc}})$ is assumed to have the form of a plane wave with energy Ω_{inc} and in-plain wave vector $k_{\mathrm{inc}}=\Omega_{\mathrm{inc}}/c\sin\vartheta$, where ϑ is the angle of incidence, $\mathcal{E}(t)$ is the electric field amplitude of the excitation pulse, which in the calculations is assumed to have a Gaussian shape with a duration of 100 fs. The summing over partial polarization P^i is introduced in Eq. (4) in order to take into account the inhomogeneous broadening of the exciton line, which is described by the distribution of $E_x^i(t)$ and A^i.

The cavity resonance energy E_{MC} and coupling constants α and β are calculated in the scattering matrix formalism[23] by solving the Maxwell equations for the particular cavity geometry and analyzing the poles of the scattering matrix in the complex energy plane.[24] Solution of Eqs. (4) and (5) gives us the dynamics of the cavity electromagnetic field $\mathcal{E}_{QW}(t)$, which depends strongly on the delay between the incident pulse $\mathcal{E}_{\mathrm{inc}}(t)$ and the exciton resonance modulation $E_X(t)$ by the strain pulse.

The temporal shape of the pulse reflected from the MC, $\mathcal{E}_{\mathrm{refl}}(t,k)$, can be found in the same resonant approximation from

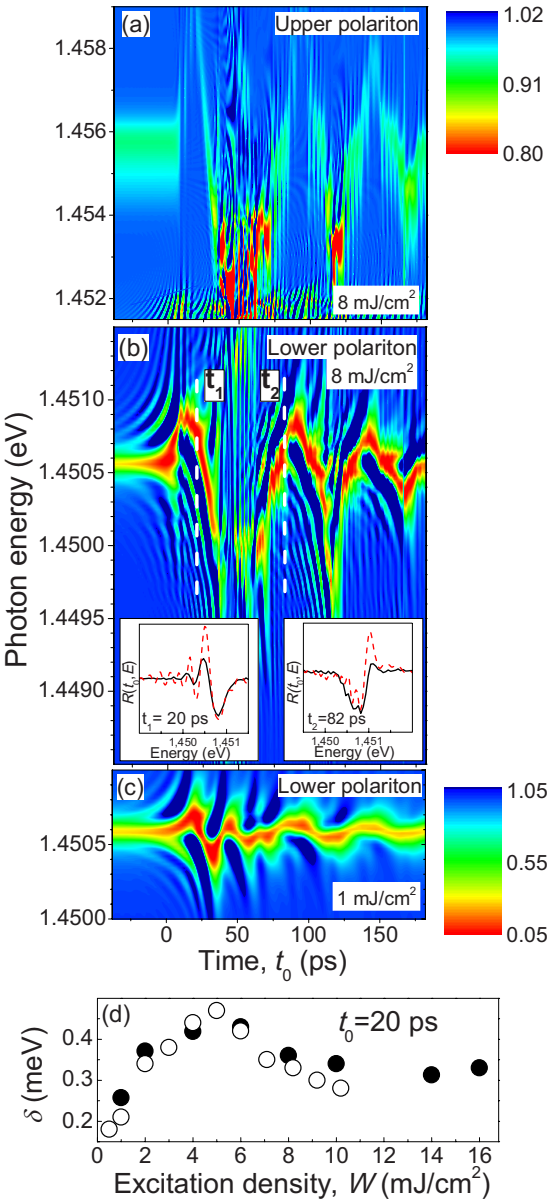

FIG. 4. (Color online) Theoretical analysis of the polariton sidebands. (a–c) Spectral/temporal contour plots of the modulated UP (a) and LP (b, c) optical signals calculated for high (a, b) and low (c) excitation densities W. Panels (b) and (c) have the same intensity scale, which is shown on the right of (c). Insets in (*b*) are normalized measured (solid lines) and calculated (dashed lines) spectral profiles obtained for two delay times t_1 and t_2. (*d*) Spectral separation δ [bar in Fig. 2(d)] between the first minimum and first maximum in the sideband spectrum of the LP modulated reflectivity signal, as measured (closed symbols) and calculated (open symbols) for $t_0=20$ ps.

$$\mathcal{E}_{\mathrm{ref}}(k,t) = \frac{\mathcal{E}_{QW}(k,t) - T^{\mathrm{inc}}(k)\mathcal{E}_{\mathrm{inc}}(k,t)}{T^{\mathrm{ref}}(k)}, \tag{6}$$

with the coefficients $T^{\mathrm{inc}}(k)$ and $T^{\mathrm{ref}}(k)$, which are calculated from Maxwell equations, depending on the microcavity design.

The temporal variation in the reflected pulse $\mathcal{E}_{\mathrm{ref}}(t,k)$ is obtained from Eq. (6) for given $\mathcal{E}_{\mathrm{inc}}(t,k)$ and $\mathcal{E}_{QW}(t,k)$, calculated from Eqs. (4) and (5) for a particular delay between $\mathcal{E}_{\mathrm{inc}}(t)$ and $E_X(t)$. The spectra of the reflected and incident pulses are obtained by Fourier transformation and the time integrated reflection spectrum is calculated as $|r(\omega)|^2 = |\mathcal{E}_{\mathrm{ref}}(\omega)/\mathcal{E}_{\mathrm{inc}}(\omega)|^2$.

The calculations have been done for the following parameters: $E_{MC}=1.4513$ eV, $\Delta E_0 = E_{MC} - E_X^0 = -3.32$ meV, $2\Omega_R = 3.26$ meV, and a Gaussian shape of the exciton line with $\Gamma_{\mathrm{nh}}=0.7$ meV as well as the center of the exciton line modulated in time by the strain pulse. In order to obtain a better fit of the reflection spectra near the upper polariton branch an asymmetric shape of the inhomogeneous exciton line was used: $A^i(E_X^i) \sim \exp\{-[(E_X^i - E_X^0)/\Gamma_{\mathrm{nh}}(E_X^i]^2\}$, with $\Gamma_{\mathrm{nh}}(E_X^i) = \Gamma_{\mathrm{nh}}\{2 + \mathrm{th}[(E_X^i - E_X^0)/\Gamma_{\mathrm{nh}}]\}$ and $\Gamma_{\mathrm{nh}}=0.7$ meV. The best agreement with experimental results has been obtained when $\tilde{a}=-20$ eV.

Figure 4(a)–4(c) shows the spectra calculated when the exciton resonance is modulated by strain pulses generated at $W=8$ mJ/cm^2 [Figs. 4(a) and 4(b)] and $W=1$ mJ/cm^2 [Fig. 4(c)]. The inhomogeneously broadened exciton line is smeared and the spectral peculiarities near the UP branch are not observed [(Fig. 4(a)]. However inhomogeneous broadening of the UP has nearly no effect on the lower branch [Fig. 4(b)] and several sidebands accompanying the main resonance are clearly visible. Most of the calculated sidebands in the LP modulated spectrum are observed also in experiment [compare Figs. 2(b) and 4(b) and see insets in Fig. 4(b)]. For quantitative comparison we chose the time interval 10 ps $< t <$ 25 ps where $\eta(t)$ changes linearly with t. To characterize the nonequidistant sideband fringes we consider the spectral separation δ [see the bar in Fig. 2(d)] between the zero-order minimum and first maximum in the sideband of the reflectivity spectrum at fixed delay t_0. Figure 3(d) shows the experimental (closed symbols) and calculated (open symbols) values of δ as function of W. These data are taken at $t_0=20$ ps where δ can be considered almost independent of t in the time interval $(t_0-\tau_c,\ t_0+\tau_c)$. Good agreement between the experimental and calculated values is seen which underlines that the suggested model of nonadiabatic optical frequency modulation is appropriate for describing the underlying physics. The nonmonotonic dependence of δ on W results from the nonlinear strain pulse propagation in the GaAs substrate.[3,10] At small $W < 3$ mJ/cm^2 the strain $\varepsilon(t)$ shows only changes in amplitude while the shape in the time interval between negative and positive $\varepsilon(t)$ remains the same. This should give $d\omega(t)/dt \sim W$ and correspondingly an increase of δ with W. For higher $W > 4$ mJ/cm^2 the dynamical strain pulse consists of an acoustic soliton train at the front and a dispersive oscillating tail at the end while in the middle $d\omega(t)/dt$ first saturates and then decreases with increasing W.[10]

V. CONCLUSIONS

In conclusion we have demonstrated experimentally the generation of sidebands in the microcavity polariton spectrum as a result of ultrafast, high amplitude optical frequency modulation. The sideband spectra show quasiperiodic fringes with a period depending on the modulation rate $d\omega(t)/dt$. The frequency modulation can be analyzed by a simple nonadiabatic model, in which the central optical frequency shifts by an amount larger than the spectral width during a time shorter than the coherence time of the resonance.

We want to point out that the origin of the detected sidebands is distinctly different from that of the well-known vibronic sidebands[25] or THz radiation induced sidebands[26] in optical spectra near the resonance lines of electron transitions. The sidebands observed in the present work require not only fast modulation times $\tau_a \ll \tau_c$ but also high modulation amplitudes $\Delta\Omega$ which exceed the stationary spectral width. The sidebands can be detected only in the coherent regime and may be considered as an optical analog of radio frequency signals for which high amplitude frequency modulation is widely used.

ACKNOWLEDGMENTS

We are thankful to P. J. S. van Capel for providing simulating results on nonlinear acoustics. This work has been supported by the Deutsche Forschugsgemeinschaft, the Russian Foundation for Basic Research, the Russian Academy of Sciences, and the Russian Ministry of Science and Technology.

[1] C. Thomsen, H. T. Grahn, H. J. Maris, and J. Tauc, Phys. Rev. B **34**, 4129 (1986).
[2] O. B. Wright, Phys. Rev. B **49**, 9985 (1994).
[3] H.-Y. Hao and H. J. Maris, Phys. Rev. B **64**, 064302 (2001).
[4] A. Bartels, T. Dekorsy, H. Kurz, and K. Köhler, Appl. Phys. Lett. **72**, 2844 (1998).
[5] C.-K. Sun, J.-C. Liang, and X.-Y. Yu, Phys. Rev. Lett. **84**, 179 (2000).
[6] M. F. Pascual Winter, G. Rozas, A. Fainstein, B. Jusserand, B. Perrin, A. Huynh, P. O. Vaccaro, and S. Saravanan, Phys. Rev. Lett. **98**, 265501 (2007).
[7] A. J. Kent, R. N. Kini, N. M. Stanton, M. Henini, B. A. Glavin, V. A. Kochelap, and T. L. Linnik, Phys. Rev. Lett. **96**, 215504 (2006).
[8] M. R. Armstrong, E. J. Reed, Ki-Yong Kim, J. H. Glownia, W. M. Howard, E. L. Piner, and J. C. Roberts, Nat. Phys. **5**, 285

(2009).
[9] N. D. Lanzillotti-Kimura, A. Fainstein, A. Huynh, B. Perrin, B. Jusserand, A. Miard, and A. Lemaître, Phys. Rev. Lett. **99**, 217405 (2007).
[10] A. V. Scherbakov, P. J. S. van Capel, A. V. Akimov, J. I. Dijkhuis, D. R. Yakovlev, T. Berstermann, and M. Bayer, Phys. Rev. Lett. **99**, 057402 (2007).
[11] L. A. Kulakova and I. S. Tarasov, JETP Lett. **78**, 67 (2003).
[12] M. M. de Lima, Jr., M. van der Poel, P. V. Santos, and J. M. Hvam, Phys. Rev. Lett. **97**, 045501 (2006).
[13] C. Weisbuch, M. Nishioka, A. Ishikawa, and Y. Arakawa, Phys. Rev. Lett. **69**, 3314 (1992).
[14] C. Weisbuch, H. Benisty, and R. Houdre, J. Lumin. **85**, 271 (2000).
[15] R. G. Brewer and R. L. Shoemaker, Phys. Rev. A **6**, 2001 (1972).
[16] G. Tas and H. J. Maris, Phys. Rev. B **49**, 15046 (1994).
[17] A. V. Akimov, A. V. Scherbakov, D. R. Yakovlev, C. T. Foxon, and M. Bayer, Phys. Rev. Lett. **97**, 037401 (2006).
[18] J. S. Blakemore, J. Appl. Phys. **53**, R123 (1982).
[19] A. Huynh, B. Perrin, N. D. Lanzillotti-Kimura, B. Jusserand, A. Fainstein, and A. Lemaître, Phys. Rev. B **78**, 233302 (2008).
[20] A. V. Scherbakov, T. Berstermann, A. V. Akimov, D. R. Yakovlev, G. Beaudoin, D. Bajoni, I. Sagnes, J. Bloch, and M. Bayer, Phys. Rev. B **78**, 241302(R) (2008).
[21] The exact value of deformation potentials for $In_{0.04}Ga_{0.96}As$ is unknown. Because of the very low In concentration we may assume that $\tilde{a}$ has a value of the same order of magnitude as the deformation potential of GaAs. For uniaxial stress along the direction (100) $\tilde{a}$ is the combination of hydrostatic and tetragonal deformation potentials for valence and conductions bands and equal to −11.5 for GaAs (Ref. 22).
[22] I. Vurgaftman, J. R. Meyer, and L. R. Ram-Mohan, J. Appl. Phys. **89**, 5815 (2001).
[23] S. G. Tikhodeev, A. L. Yablonskii, E. A. Muljarov, N. A. Gippius, and T. Ishihara, Phys. Rev. B **66**, 045102 (2002).
[24] N. A. Gippius, S. G. Tikhodeev, and T. Ishihara, Phys. Rev. B **72**, 045138 (2005).
[25] K. Rebane, *Impurity Spectra of Solids* (Plenum Press, New York, 1970).
[26] J. Kono, M. Y. Su, T. Inoshita, T. Noda, M. S. Sherwin, S. J. Allen, Jr., and H. Sakaki, Phys. Rev. Lett. **79**, 1758 (1997).